Tong, Zhen and Luo, Xichun and Jiang, Xiangqian and Bai, Qingshun and Xiu, Zongwei and Blunt, Liam and Liang, Yingchun (2016) Review on FIB-induced damage in diamond materials. Current Nanoscience, 12 (6). pp. 685-695. ISSN 1573-4137 , http://dx.doi.org/10.2174/1573413712666160530105707

This version is available at https://strathprints.strath.ac.uk/61090/

Strathprints is designed to allow users to access the research output of the University of Strathclyde. Unless otherwise explicitly stated on the manuscript, Copyright © and Moral Rights for the papers on this site are retained by the individual authors and/or other copyright owners. Please check the manuscript for details of any other licences that may have been applied. You may not engage in further distribution of the material for any profitmaking activities or any commercial gain. You may freely distribute both the url (https://strathprints.strath.ac.uk/) and the content of this paper for research or private study, educational, or not-for-profit purposes without prior permission or charge.

Any correspondence concerning this service should be sent to the Strathprints administrator: strathprints@strath.ac.uk

The Strathprints institutional repository (https://strathprints.strath.ac.uk) is a digital archive of University of Strathclyde research outputs. It has been developed to disseminate open access research outputs, expose data about those outputs, and enable the management and persistent access to Strathclyde's intellectual output.

Review on FIB-induced damage in diamond materials

Zhen Tong[1, 2]*, Xiangqian Jiang[2], Xichun Luo[3], Qingshun Bai[1], Zongwei Xu[4], Liam Blunt[2], Yingchun Liang[1]

1 Center for Precision Engineering, Harbin Institute of Technology, Harbin 150001, China

2 Centre for Precision Technologies, University of Huddersfield, Huddersfield HD1 3DH, UK

3 Department of Design, Manufacture & Engineering Management, University of Strathclyde, Glasgow G1 1XQ, UK

4 Centre of MicroNano Manufacturing Technology, Tianjin University, Tianjin 300072, China

**Corresponding email: zhen.tong528@gmail.com; z.tong@hud.ac.uk*

Tel.: +86 0451 86402682; Fax: +86 0451 86402681.

Abstract: Background: Although various advanced FIB processing methods for the fabrication of 3D nanostructures have been successfully developed by many researchers, the FIB milling has an unavoidable result in terms of the implantation of ion source materials and the formation of damaged layer at the near surface. Understanding the ion-solid interactions physics provides a unique way to control the FIB produced defects in terms of their shape and location.

Methods: We have carefully selected peer-reviewed papers which mainly focusing on the review questions of this paper. A deductive content analysis method was used to analyse the methods, findings and conclusions of these papers. Based on their research methods, we classify their works in different groups. The theory of ion-matter interaction and the previous investigation on ion-induced damage in diamond were reviewed and discussed.

Results: The previous research work has provided a systematic analysis of ion-induced damage in diamond. Both experimental and simulation methods have been developed to understand the damage process. The damaged layers created in FIB processing process can significantly degrade/alter the device performance and limit the applications of FIB nanofabrication technique. There are still challenges involved in fabricating large, flat, and uniform TEM samples in undoped non-conductive diamond.

Conclusions: The post-facto-observation leaves a gap in understanding the formation process of ion-induced damage, forcing the use of assumptions. In contrast, MD simulations of ion bombardment have shed much light on ion beam mixing for decades. These activities make it an interesting and important task to understand what the fundamental effects of energetic particles on matter are.

Keywords: focused ion beam; ion irradiation damage; diamond; TEM; molecular dynamics; ion bombardment.

1 Theory of ion matter interaction

When an energetic ion strikes the matter, the ions lose energy immediately by means of both nuclear and electronic interactions with the substrate atoms transferring energy and momentum. The primary nuclear interactions lead to the displacement of the target atoms from their original positions and the creation of vacancies in the target material if the transferred energy exceeds the target atomic-mass-dependent and angular-dependent displacement energy E_d. If the energy transferred to the primary atom 'knocked on' is sufficiently high, the secondary, tertiary and higher order atomic knock-ons take place which refers to the energetic atomic collision cascade as schematically shown in figure 1. The displaced atoms may run out from the surface which is known as sputtering. The implantation of the incident ions and the process of vacancy-interstitial creation lead to the disorder of the local crystal structure in terms of condensed matter phase transition, amorphization, swelling and/or other physical changes depending on the type of target material as well as the ion beam processing parameters.

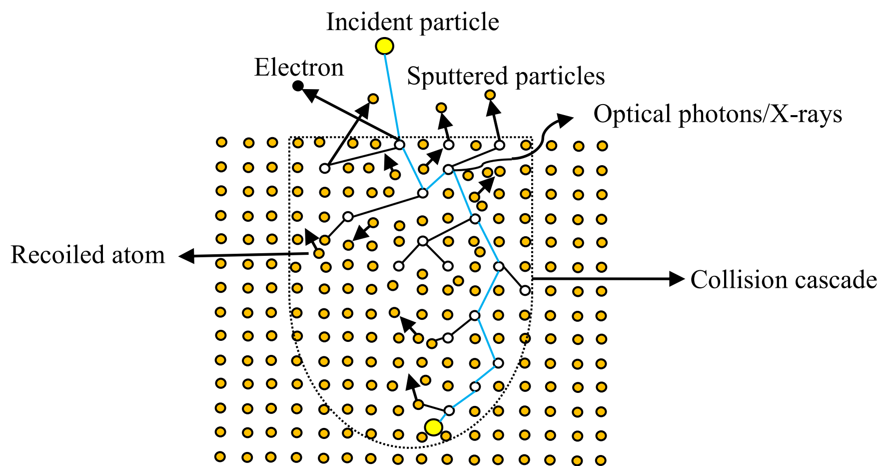

Figure 1: Schematic diagram of the various processes that occur during ion-material interaction.

Briefly the mechanism operating to slow down incident ions and to dissipate ion energy can be classified into three categories: elastic collisions process (nuclear stopping), inelastic

collision process (electronic stopping), and charge exchange process. The energy loss process can be expressed as:

$$\left(\frac{dE}{dX}\right)_{loss} = \left(\frac{dE}{dX}\right)_{Elect} + \left(\frac{dE}{dX}\right)_{Nucl} + \left(\frac{dE}{dX}\right)_{ChargeExchange} \quad (2\text{-}1)$$

where $\left(\frac{dE}{dX}\right)_{Elect}$ is loss due to electron, $\left(\frac{dE}{dX}\right)_{nucl}$ is loss due to neutron, and $\left(\frac{dE}{dX}\right)_{ChargeExchange}$ is loss due to charge exchange. Since charge exchange loss represents a small fraction of total energy loss for low charged ions, it can be neglected.

The nuclear energy transfer occurs in discrete steps as a result of elastic collisions where the energy of the incoming ion is lost to target atoms by momentum transfer. The electronic energy loss occurs as a result of inelastic scattering events where the transfer of energy occurs through electronic excitation.

Figure 2 shows the electronic and nuclear stopping curves for Ga ion in single crystal diamond calculated by SRIM [1] software. At low energy regime the stopping power is proportional to the velocity of the ions. The nuclear energy loss attains a maximum value (around 50 keV) and gradually decreases with the incident energy. However, for the high-energy regime the electron energy loss dominates the energy transfer process because the velocity of the incoming ion becomes comparable to that of the orbital electrons. For material removed by the collision cascade, the optimized energy is normally in a range of 10–100 keV [2]. The electron energy loss is smaller than the nuclear energy loss and hence it has a negligible contribution to the energy transfer in low-energy regime.

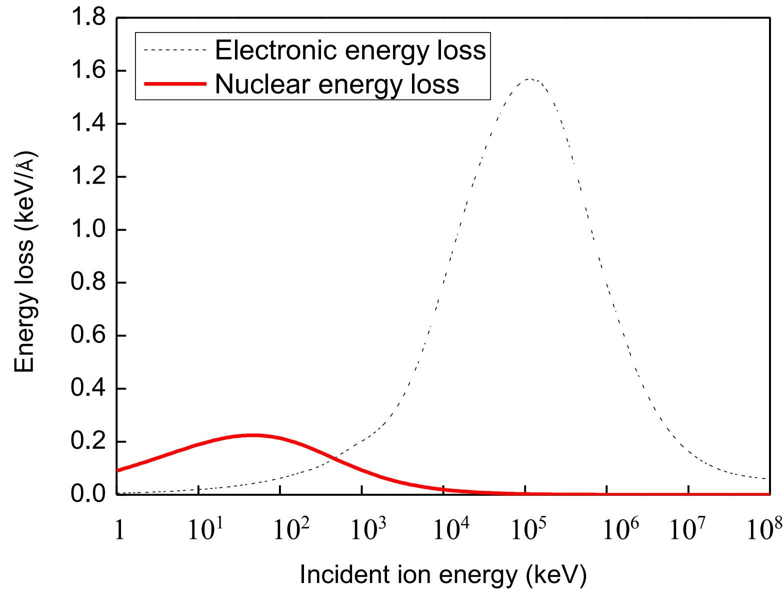

Figure 2: The electronic and nuclear stopping curves for Ga ion in single crystal diamond calculated by SRIM (using 52 eV for the displacement energy).

2 Experimental study on FIB-induced damage in diamond

In recent decades, a variety of techniques including Raman spectroscopy [3, 4], optical measurements [5], atomic force microscopy (AFM) [6, 7], scanning electron microscopy (SEM) [7], and transmission electron microscopy (TEM) [8-10] have been developed to investigate the ion-induced damage in diamond substrates caused by gammas[11], neutrons[12], electrons [13], protons [14] and ions [8-10] under different scale of energies. There is also a body of work looking at the radiation hardness of diamond in particle detectors for use in high-energy physics, nuclear and medical applications [15-17]. However, due to the inherent differences in the beam species and energies, there are remarkable differences in the characteristics of ion-induced damage when using different kinds of ion beams. Since the commercial LMIS based Ga^+ FIB beam normally has a voltage ranging from 2 kV to 30 kV, the ion-solid interaction in a typical FIB milling process is governed by the nuclear energy loss at the surface of the solid [18].

2.1 Formation of a-C and the required critical dose

In typical LMIS based Ga^+ FIB beam milling process, the energy transferred by the incident Ga^+ is usually sufficient to break the C-C bond leading to the displacement of lattice atoms, surface sputtering and creation of craters and hillocks, formation of point defects, and the initiation of other secondary processes. These dynamic effects are transient. The displaced atoms may partly re-order into different characteristic arrangements of atoms when the density of point defect is sufficient high. A residual damaged layer is then formed at the near surface comprised mostly of vacancies and interstitials.

Admas *et al*. [19] has used TEM to study the amorphous carbon (a-C) layer in diamond created by FIB milling. The thickness of the a-C layer varies at different sites on rough surfaces, and a larger amorphous layer was found when a small local incident angle of ion beam was applied. A 20% reduction in the thickness of a-C layer was found when using H_2O assisted FIB milling [19], indicating that a reactive sputtering during the H_2O assisted FIB milling process can suppress the formation of damaged layer.

Brunetto *et al*. [4] studied the ion-induced amorphization of diamond (CVD diamond) by in-situ Ramon spectroscopy. The energies of impact ions (H^+, He^+, and Ar^+) ranging from 30 keV up to 200 keV were used. Amorphous carbon was formed when a threshold of damage density of 2.0×10^{22} vacancies/cm^3 was reached. In order to further determine the amorphization threshold for ion implantation in diamond, Rubanov *et al*. [9] investigated the ion-induced damaged layers in a synthetic type1b diamond substrate under eight different ion doses via a combination of cross-sectional TEM imaging and electron energy loss spectroscopy (EELS) analysis. The ion dose ranges from 6.0×10^{14} to 1.0×10^{16} ions/cm^2. Their results show that amorphization threshold for ion implantation in diamond at room temperature was determined to be 5.2×10^{22} vacancies/cm^3. The thickness of the damaged layer grew with the ion dose and achieved an equilibrium value of 44 nm for continuous 30 keV Ga^+ FIB milling [9].

Mckenzie *et al*. [8] studied the FIB irradiation of a single crystal natural conductive diamond

under 30 keV Ga^+ focused ion beam through scanning transmission electron microscopy (STEM), EELS, and electron backscattered diffraction (EBSD). The results show that the near surface microstructure varied with the increase of ion dose. The critical dose for the amorphization of the diamond substrate was found to be 2.0×10^{14} ions/cm^2. A stable amorphous layer (thickness of 35 nm) was found at a high dose (1.0×10^{15} ions/cm^2). The hydrogen and oxygen contents were found within the amorphous carbon layer [8].

Most recently, Tong et al. [20] carried out a series of TEM inspections to measure the FIB-induced damage layer in a single crystal diamond tool under different FIB beam voltages 8 kV, 16 kV and 30 kV (figure 3). They characterized the FIB-induced damage layer using a FEI Nova 200 nanolab dual beam FIB system which point resolution is 2.4 nm and line resolution is 1.5 nm. The results indicated that during FIB processing cutting tools made of natural single crystal diamond, the energetic Ga^+ collision will create an impulse-dependent damage layer at the irradiated surface. For the tested beam voltages in a typical FIB system (from 8 kV to 30 kV), the thicknesses of the damaged layers formed on a diamond tool surface increased from 11.5 nm to 27.6 nm. The research findings provided the in-depth understanding of the wear of nanoscale multi-tip diamond tools which has been observed in [21]. Because the macroscopic and microscopic properties of the amorphous carbon are quite different from the diamond bulk, this damaged layer (doping with implanted Ga) would get wear first during the nanometric cutting. A lower sputtering energy and post ion polishing process were suggested in the FIB-based nanoscale tool fabrication process to improve the tool life by minimizing/removing the surface residual a-C layers.

From the research work discussed above, it is also noted that the threshold value of ion dose between the nature single point diamond and synthetic diamond such as CVD diamond are quite different. This is mainly because of the difference in the density of these two kinds of diamond materials. The thickness of a-C layer was found to mainly depend on the beam voltage, the sputtering environment and the surface tomography of diamond. The anisotropy of diamond materials and big challenge of TEM sample preparation also bring research

difficulties in exploring the full map of FIB-induced damage in diamond.

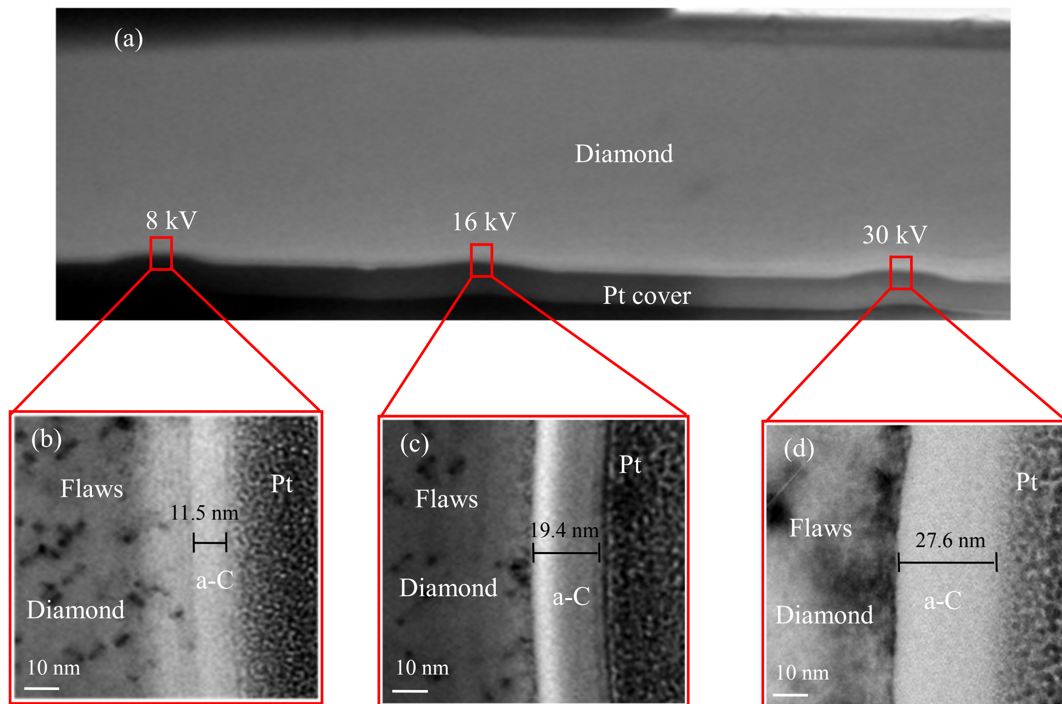

Figure 3: EFTEM images of the ion-induced damage areas. (a) The TEM sample after thinning; (b)-(d) are the EFTEM images showing the ion-induced damage layers formed under beam voltages of 8 kV, 16kV, and 30kV, respectively [20].

2.2 Effect of implantation of Ga

Apart from the amorphization in diamond, there are additional effects which are caused by the implantation of ion source atoms. For example, adding of ion species into the sample can change the chemical composition, optical, magnetic, electrical, and mechanical properties of FIB fabricated products.

Gnaser and co-workers [22] reported a fluence-dependent evolution of the implanted Ga concentration in nanocrystalline diamond films by SIMS. A linear increase of the Ga peak concentration with fluence was found up to ~2.0×10^{16} ions/cm^2 and the Ga content approached a saturation level at about 2.0×10^{17} ions/cm^2. Hamada *et al.* [15] reported that the accumulation of implanted gallium ions would degrade the stability of applicable electric field of micro structures fabricated in an undoped diamond substrate. A combination of high

temperature annealing in high vacuum with a following chemical treatment with acid and alkaline solutions can effectively remove the implanted Ga atoms. Similarly, Philipp *et al*. [23] observed Ga segregation in FIB modified tetrahedral amorphous carbon (ta-C) films. The implanted Ga was segregated at ta-C surface due to the phase separation of Ga and C. The Ga droplets were transformed into spherical shaped dots at a high temperature (above 300 °C). The size and the height of Ga dots segregated on the surface increased with the increase of annealing temperature. Unocic and co-workers [24] studied the effects of gallium focused ion beam milling on preparation of aluminium thin foils and identified that the implanted gallium will concentrate on the surface, grain boundaries and interphase boundaries of sample (figure 4). Low-energy Ar ion nanomilling is potentially can be used for removing gallium implantation layers of aluminium thin foils. Kupfer *et al*. [25] proposed a FIB-only approach for the fabrication of diamond micro-cantilevers and pointed out that the contamination with the gallium ions in diamond can be effectively eliminated by high temperature thermal treatment (above 500 °C).

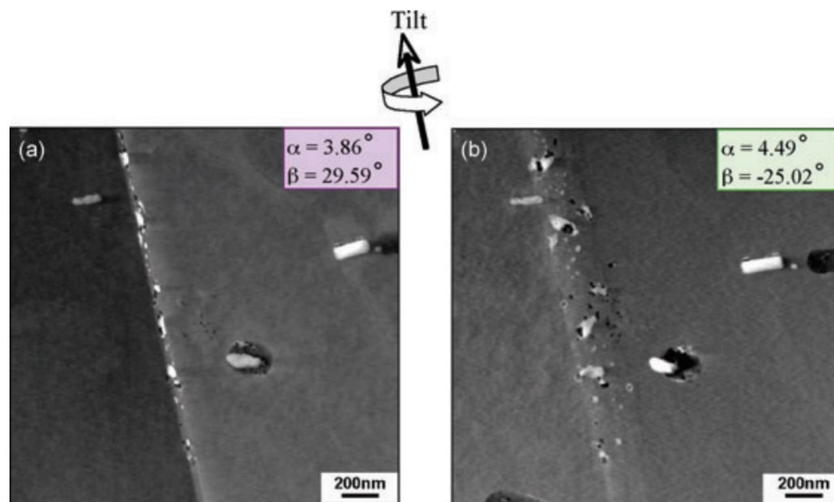

Figure 4: DF STEM micrographs showing the presence of distinct gallium clusters within grain boundaries distributed in discontinuous manner along a grain boundary viewed in (a) edge-on and (b) inclined orientations [24].

Recently, Xu *et al*. [26] investigated the FIB-induced damage in diamond tool used in nanometric cutting and reported that the tool wear may result from the a-C layer created

during FIB milling process. Through MC simulation, they pointed out that decreasing the FIB processing energy can reduce the Ga^+ implantation depth as well as the thickness of a-C layer. Kawasegi *et al*. [27] reported that the doping of gallium ion in a diamond tool (type 1b (1 0 0)-oriented single crystal diamond) can increase the adhesion of work materials to the tool surface, which would result in a rapid diamond tool wear at the gallium rich area. A combination of 500 °C heat treatment and aluminium deposition layer was demonstrated to be an effective method to eliminate the non-diamond phase of the FIB irradiated diamond surface and results in the improvements in terms of tool life and the surface quality and accuracy of the machined part. Additionally, Buckmaster and co-workers [28] has taken the advantages of Ga accumulation to fabricate nanodots by spatially controlling Ga implantation into SiO_2 using a FIB followed by vacuum annealing (as shown in figure 5). These nanodots can be potentially used as Ga-based semiconductor quantum dots and also as a catalyst for nanowire growth.

(a)

(b)

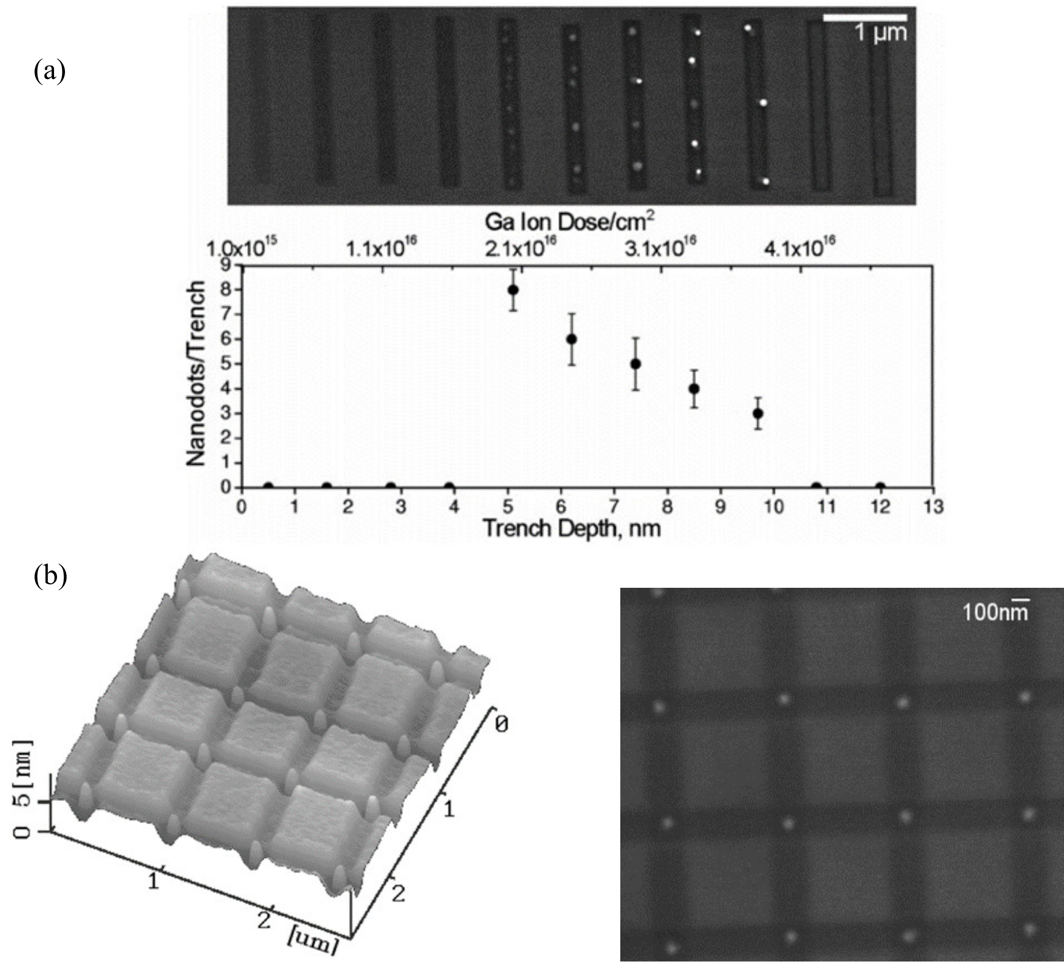

Figure 5: (a) SEM image of 200 nm by 2 μm trenches patterned by systematically increasing the Ga doses for each trench show a critical Ga dose for nucleation and also a linear decrease in the average number of nanodots (average of three identical sets of patterns) per trench with increasing dose; (b) the AFM and SEM images of an array of self-assembled capped Ga nanodots formed at the intersection of 2.5 nm deep FIB patterned trenches [28].

3 Atomistic simulations of ion bombardment

In order to probe areas outside the range of the experimental observation, different kinds of computer simulation methods have been developed to examine the mechanism of ion penetration and ion-induced damage in various materials. Binary collision approximation (BCA) and molecular dynamics (MD) are the two major simulation methods.

In both BCA and classical MD simulations the interactions between atoms in the sample are

described by interatomic potentials. The essential difference between these methods is how the atom motion is considered. BCA method approximates the full atomic dynamics of a material by a series of binary collisions. It provides a computationally efficient means for examining the transport of energetic ions by neglecting many possible body effects[1, 29]. MD methods describe the interactions between atoms involved in ion collision process more realistically, requiring much larger amounts of computer capacity than the BCA method [30]. The forthcoming sections will point out the principle and problems of BCA simulations in calculating ion collision, and illustrate why MD method is suitable for the study of energetic ion bombardment events by reviewing the significant results obtained from typical MD simulations.

3.1 Binary collision approximation method

In BCA calculations the movements of incident particles are usually treated as a sequence of independent binary collisions. For each individual collision the classical scattering integral is solved for a given impact parameter between the moving atom and a stationary atom in the target material by numerical integration [31]. The impact parameters of the next colliding atom and the atomic type used in the scattering integral are determined either from a stochastic distribution (such as the Monte-Carlo algorithm used in programs like TRIM/SRIM[1, 32], or in a way that considers the crystal structure of the matter (such as the method used in MARLOWE [33] and Crystal-TRIM [34, 35] where the atoms are either frozen at the ordered lattice sites or oscillating with the Debye frequency). Because the solution of the integral of motion results in precise scattering angles for both the projectile and the target atoms, as shown in figure 6, a fairly reliable prediction of ions penetration depths and formation of point defects in implanted materials can be achieved for almost all cases of interest. Owing to its high computational efficiency in defect cascade simulations, it stands as a significant method particularly for calculating high-energy (MeV) ion behaviour [36]. Most recently, in the newly reported multiscale scheme, the BCA method can be used

combined with MD simulations to include multiple scales in dimensions during high energy ion irradiation [37, 38].

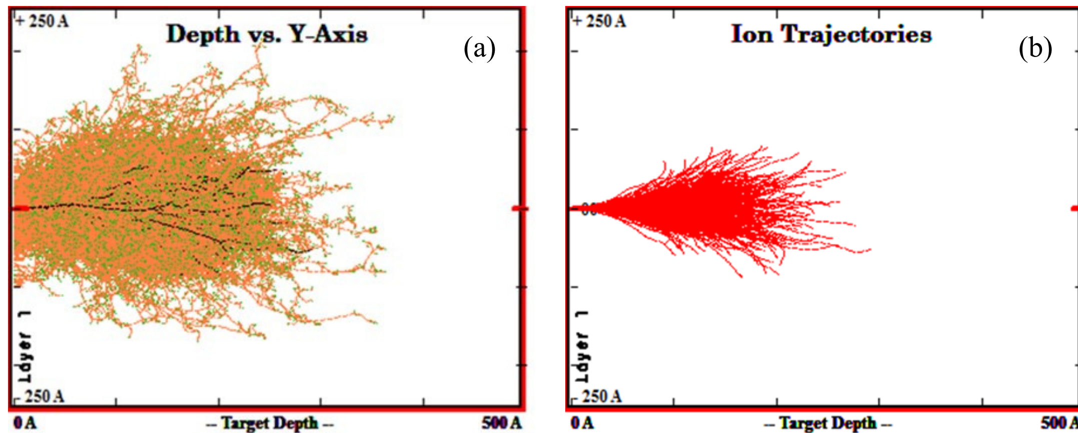

Figure 6: The TRIM simulation results of 30 keV Ga ion sputtering single crystal diamond process. (a) the trace of implanted Ga particles; and (b) the distribution of residual damage layer. (Displacement energy 50 eV, lattice binding energy 3 eV, surface binding energy 7.5 eV)

Nevertheless, the BAC method has some inherent obstacles in describing the slowing-down process of energetic ions realistically. The first and the most important one is the basic assumption of binary collisions when trying to build a model taking multiple atomic interactions into account. It also makes it impossible to distinguish a cascade when it goes from the linear cascade to the heat spike regime [22, 36]. The scattering integral also does not allow for incorporating angle-dependent potentials, which significantly limits its capacity to describe covalently bonded materials like silicon and diamond [30, 39]. Moreover, although basically BCA models can estimate the overall spatial distribution of vacancy-like and interstitial-like damage by counting recoils that exceed the threshold displacement energy, it cannot distinguish the atomic structure of these defects [40]. In some cases, the defect distribution information can be irrelevant or meaningless. For example, the BCA simulation is able to predict the production of point defects in diamond created by the heavy ion irradiation. However, it is not able to pinpoint the location of a vacancy or interstitial in an amorphous zone and cannot identify whether local phase transition takes place. Additionally, the algorithm describes the atoms binding at surface in the same way as the inside atoms.

Therefore, it is problematic when describing the sputtering or other surface effects [41]. In contrast, MD simulation which can describe the non-equilibrium ballistic motion of high energy ions as well as the subsequent thermalization of the ions is ideally suited for the modelling of ion bombardment, and have emerged as the main computational tool for the study of irradiation effects [42].

3.2 MD modelling of ion bombardment

In MD simulation, movements of all atoms are calculated. The full many-body dynamics in an atomic system is simulated with the accuracy limited only by the reliability of the interaction Hamiltonian employed [29]. The time evolution of an atomic system is calculated by numerically solving Newton equations of motion in a step-by-step fashion.

In fact, since MD developed as a technique in the 1950s, it has been used to study the irradiation effects such as the phase transitions in hard spheres system [43], the thermal spike in irradiated metals [44], and many-processes in an energetic displacement cascade [45]. The major boom in MD simulations begins in the 1980s when the computer capacity was sufficient to monitor a system of thousands of atoms. Harrison *et al*. [46] carried out MD simulations to investigate the sputtering of metals and rare gases, and initially revealed the channelling and blocking mechanisms for ion stopping and the emission patterns of particles from single crystals. Rubia *et al*. [47] built a large scale MD model to fully contain the collision cascade and demonstrated the existence of the local melting in copper cascades created by 3 keV and 5 keV collisions. In the mid-1990s, numerous studies examined the defect and dislocation production in collision cascades [45, 48, 49] and illustrated local melting in a large variety of other materials [50, 51].

In addition to the thermal spike and its effect, other aspects such as the formation of defects, their spatial configuration and properties, and the phase transformations have also been investigated. A distinct mechanism of atom mixing in a displacement cascade, such as recoil implantation, cascade mixing, and thermal spike mixing was schematically shown in figure 7.

It is reported that the cascade mixing theory yields reasonable agreement with experiment, however, the mixing value is far too small for those materials where thermal spikes are important [45]. Ghaly *et al*. [52] further pointed out that the formation mechanism of damage product at near surface was different from those in the bulk.

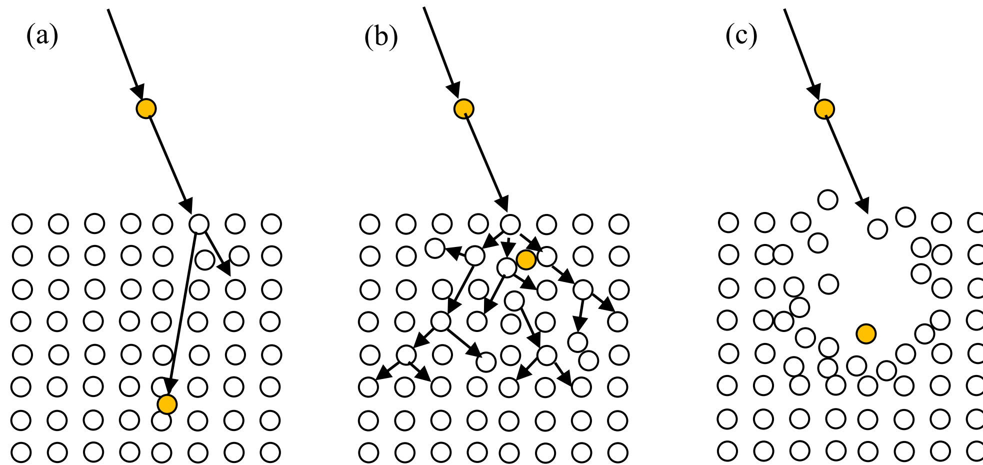

Figure 7: Schematic depiction of the three mechanisms of ion beam mixing: (a) recoil implantation; (b) cascade mixing, and (c) thermal spike mixing.

Moreover, the motion and clustering of vacancies and interstitials [53], annealing [54] during the formation process of the stable amorphous zone in a collision cascade has also been studied by MD simulations. In contrast to the annealing effects observed for FCC (face-centred cubic) metals where both interstitials and vacancies were pushed toward the centre of the liquid region, in silicon the amount of new damage created by a cascade is roughly independent of the number of initial point defects (as shown in figure 8). The amorphization of Si under low-energy recoils (about 3–15 eV) can also lead to a significant thermal dynamic recrystallization component during ion irradiation [55].

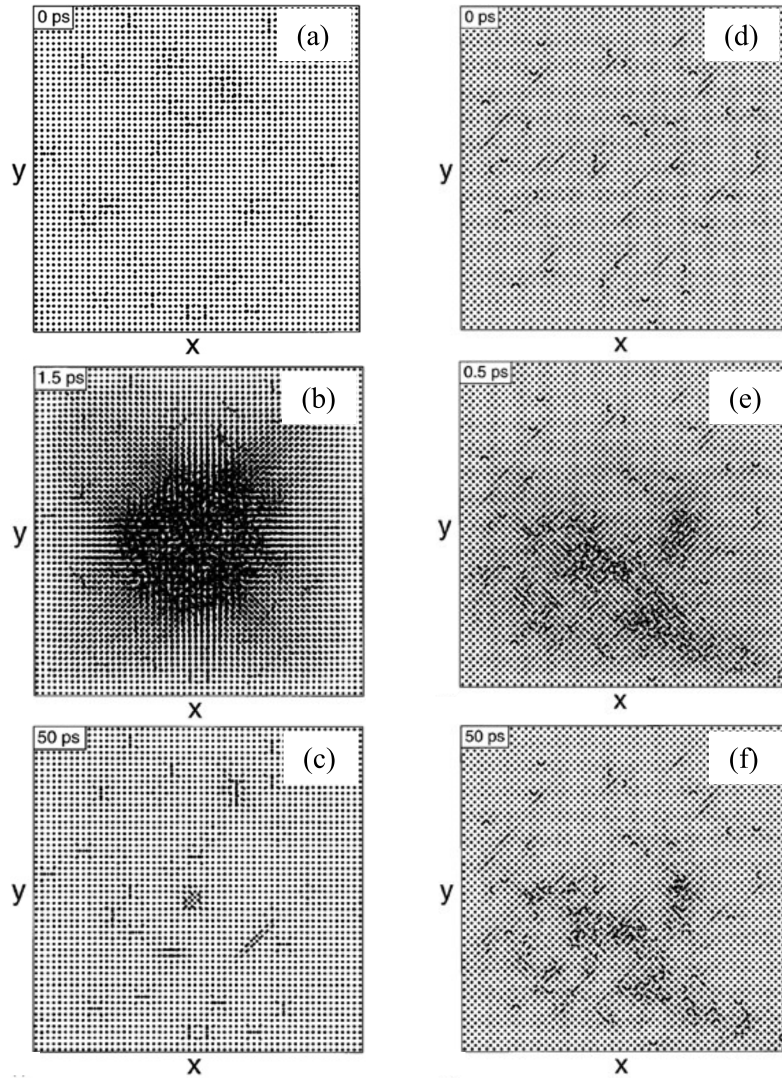

Figure 8: Snapshots of a 5 keV Au cascade (left column), and Si cascade (right column. The cascade is clearly less dense and well defined than in gold, and much more damage remains afterwards [54].

These research works contributed a lot towards the understanding on the fundamental processes of ion-induced defects production. However, the spatial and time scales of these early models were too small to fully track the whole process of multi-particle collision. The rapid progress in developing the computer power capacity in recent years, especially the development of parallel computing cluster technique, has largely increased the size of computing domain and enabled the promised elucidation of multi-particle ion collision processes. Since then many research papers started to address the damage creation in various

target materials under different irradiation conditions.

Kalish and his co-workers [56, 57] simulated the ion-induced damage in diamond and the thermal annealing process. The disrupted region (amorphous carbon) was rich in sp^2-like (graphitic) bonds, and the <1 0 0> split interstitial with a bonding configuration resembling graphite was found to be the most stable defect (figure 11). The phase transformation between sp^2-bonded and sp^3-bonded Carbon atoms depended significantly on the density of point defects created by the implantation levels [58, 59]. The damaged region collapses to graphite when the vacancy density exceeds a critical density of vacancies, whereas it regrows to diamond structure upon annealing for lower damage levels [58, 59].

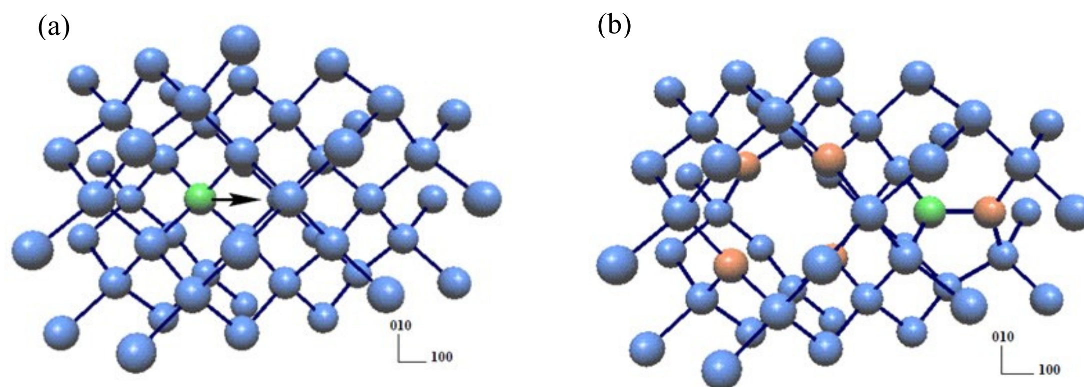

Figure 9: (a) Structure of the sample before any displacement (The direction of displacement is indicated by the arrow). (b) Structure of the damaged area obtained from knocking the marked (in green) atom with energy of 60 eV. Atoms remaining sp^3 bonded are drawn in blue. The displaced atom, now a member of a split interstitial is drawn in green, and sp^2 bonded atoms are drawn in brown [56]. (Reproduced under the permission from Copyright© 2016 World Scientific Publishing Co Pte Ltd)

Satake *et al.* [60] studied the influence of computational domain and empirical potential function on the accuracy of simulation results (40 keV Ga^+ impact silicon). The results show that a combination of ZBL (Ziegler, Biersack and Littmark) and Tersoff potential functions can offer more accurate description of the collision process than other tested potentials. They further studied the effect of ion influence on the hillock structure (as shown in figure 10) [61].

Li *et al.* [62] compared the structural change of amorphous carbon when using different potential functions and recommend Tersoff potential for modelling ta-C. Large-scale MD computational domain was reported to be able to help express accurately the stopping of incident ions [60] as well as the fully track of thermal spike [63].

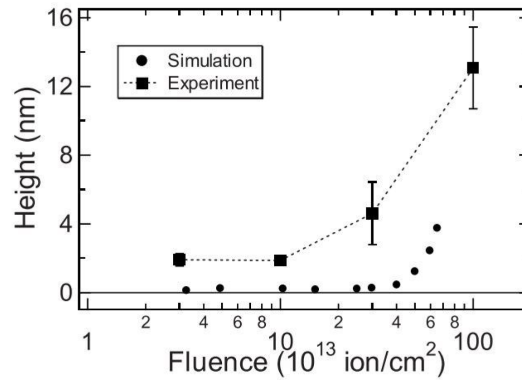

Figure 10: Effect of ion influence on the hillock structure [61].

Most recently, many research works were focused on the influence of beam processing parameters on the structure and properties of irradiated materials. Some recent research work also reported the effects of ion fluence and acceleration energy of incident ion on the Si surface deformation as shown in figure 12 [61, 64]. Li and co-workers [65] studied the effect of incident angles of energetic carbon atoms (0-60°) on the structure and properties of diamond-like carbon (DLC) film. The surface roughness and the porous structure were increased with the incident angle. A significant reduction of residual compressive stress was found when an incident angle of 45° was used, implying the great potential of controlling incident angle to improve the adhesive strength of DLC film.

3.3 Key parameters in MD simulation of ion bombardment

The ion spatial discription, boundary conditions and potential functions are the key parameters for a successful MD simualtion of ion bombardment. According to the ion spatial distribution, the ion collision model can be broadly classified into indirect collision model (figure 11(a)) and direct ion collision model (figure 11(b)). For indirect collision model, the spatial distributions of impact ions are not considered. The ion source material is usually the

same as the substrate material. The ion collision was performed as a local heating spike[66] or sudden shaking of the atoms at collision centre[54, 67]. These kinds of models have advantages when describing the thermal spike and the recrystallization of atomic defects during ion irradiation processes. However, it is quite difficult to describe the whole process of the FIB milling process such as the sputtering and ion pulse related phenomenon.

In contrast, the direct collision model proposed by some researchers [20, 61, 68] recently were able to describe the whole collision process considering the spatial distribution of impact particles and the interactions between the incident particles and the workpiece atoms. In these models, the ion fluence was calculated as the number of collision atoms from the irradiation area. Thus, the results predicted by these kinds of models can be compared with experimental results potentially. However, the difference in the time scale is a big challenge for a quantitative comparison between the experimental and simulation results.

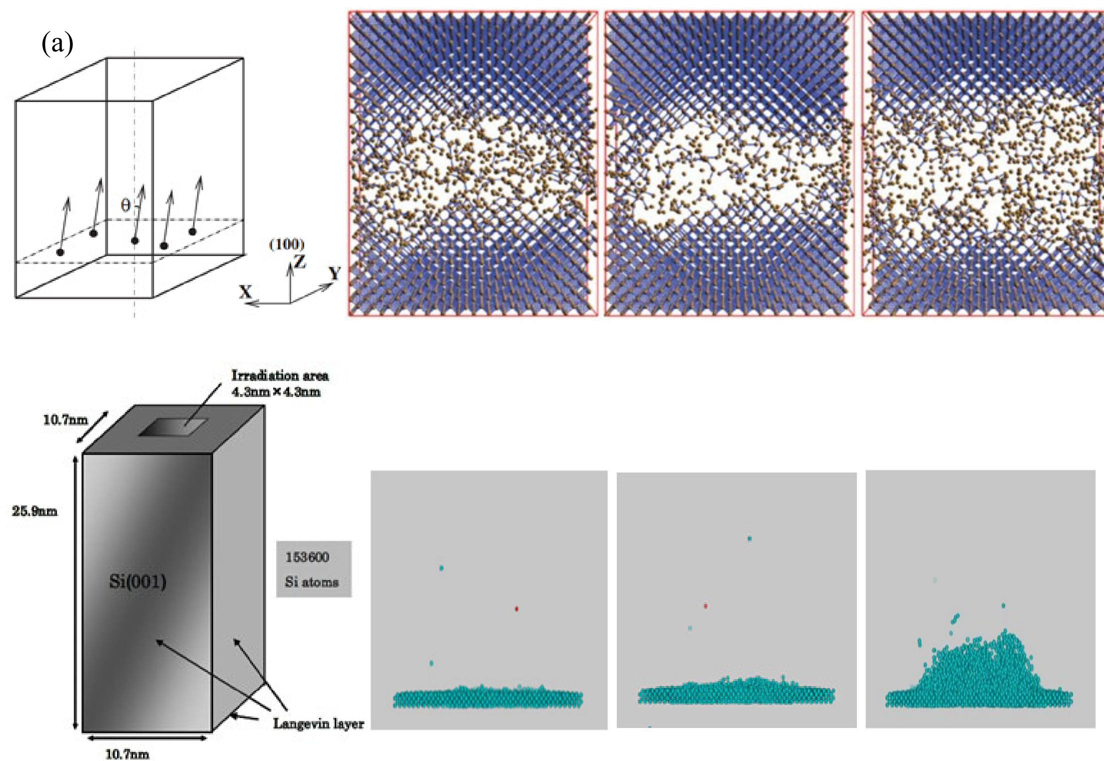

Figure 11. MD simulation models for ion irradiation. (a) Indirect collision model and the residual defects in diamond [67]; (b) Direct ion collision model and the sputtering process of Si [61].

MD simulations are usually carried out in a 3D cubic box having three different zones:

boundary atoms zone, thermostatic atoms zone, and Newton atoms zone. The boundary atoms are kept fixed in their initial lattice positions, serving to maintain the symmetry of the lattice. The thermostatic atoms are used to simulate the thermostatic effects of the bulk and guarantee the equilibrium temperature to approach a desired value. The workpiece is represented by the Newton atoms which are assumed to follow the classical Newton's second law of motion, computed from the interatomic forces described by potential functions.

For the energetic ion collision process, it is important to make sure that the system size is able to track all the stopping processes of incident particles as well as the entire collision cascades happening subsequently. In a typical FIB machining process, each incident Ga ion will create a damaged region along its trajectory in the target material. As a result, small systems cannot be used in a full analysis of collision cascades, and the thickness of the substrate built in a MD system needs to be large enough for multi-particle collisions. Recently, Smith *et al.* [63] pointed out that there is no fixed rule for boundary condition and system size as long as the lateral cascade never reaches the edges of the system. Thus, the boundary influence is negligible when the boundary atoms are sufficiently far away from the cascade. Since the kinetic energies of incident ions and the properties of target materials are the two major impact parameters determining the actual range of collision cascades, the system size and the boundary condition should be calculated by a numerical experimentation.

Moreover, the accurate level of MD simulation results depends significantly on the selected potential function. The potential function in an MD simulation is a description of the terms by which the particles in the simulation will interact. In recent decades, many empirical and semi-empirical potential functions have been developed to approximate atomic force fields for large atomic aggregates. According to the number of atoms considered in computing the interaction atomic forces, the potential functions can be broadly classified into pair potential functions and many-body potential functions. The pair potential functions only consider interactions between the particles of the system in pairs. The classic examples of such pair potential functions are the non-bonded Lennard-Jones potential function [69, 70] and the

Morse potential function [71, 72]. The many-body potential functions include the effects of three or more particles interacting with each other. An example of such a potential for covalent materials is the Tersoff potential function [73]. Other examples are embedded atom method (EAM) potentials [74] and Tight-Binding Second Moment Approximation (TBSMA) potentials [75] which are widely used to describe ductile metals and alloys.

Table 1 lists the potential functions used in the MD simulation studies of energetic ion collisions performed so far with highlighting remarks. Various potential functions have been developed and used in the previous research works. Most recently, Satake *et al.* [60] compared the influence of potential functions on the energy transition and indicated that a combination of the Tersoff potential with the ZBL potential (named Tersoff.ZBL potential) has the best results among other tested potential functions.

Table 1: Main potential functions for the simulation of ion collision

Case (Ion source/Workpiece)	Potential function for Ion-workpiece	Potential function for workpiece-workpiece	Details
Ga/Si	Lennard-Jones	Tersoff	S. Satake *et al.* [60]
Ga/Si	Tersoff	Tersoff	
Ga/Si	ZBL	Tersoff	
Ar/Si	ZBL	Tersoff	S. Satake *et al.* [61]
Ar/4H-SiC	ZBL	Tersoff	S. Satake *et al.* [76]
Ga/Si	Tersoff.ZBL	Tersoff.ZBL	A. Burenkov *et al.* [77]
Ga/Si	ZBL	Tersoff.ZBL	M.F. Russo Jr. *et al.* [78]

Considering the factors discussed above, Tong *et al.* [20, 68] developed a multi-particle large-scale ion collision model to study the dynamic creation of atomic defects leading to the amorphization of single crystal diamond under different beam voltages (figure 12). The spatial distribution of Ga^{+} was considered as random distribution with a circular cross section above the diamond substrate. A single ion collision model was built to obtain necessary

parameters for building the multi-particle ion collision model, for example the minimum time step, the size of the simulation box, the time of relaxation process required between each ion collision etc. The Ga stroked the diamond substrate one by one. The formation of atomic defects, the thermal spike and the recrystallization of atomic defects have been observed during each single ion collision process (figure 13). Moreover, the results showed that the defects created inside diamond matrix increased with the increase of ion dose and approaching a stable value. When the material removal rate reaches the damage formation rate, a stable a-C layer is likely to be obtained. This ion-induced dynamic equilibrium damage process in diamond found in simulations was qualitatively supported by the ion fluence-dependent amorphization of diamond substrate observed in previous experiments[8, 22]. The thickness and the amorphization level of the dynamic equilibrium damage layer depend significantly on the applied beam voltage.

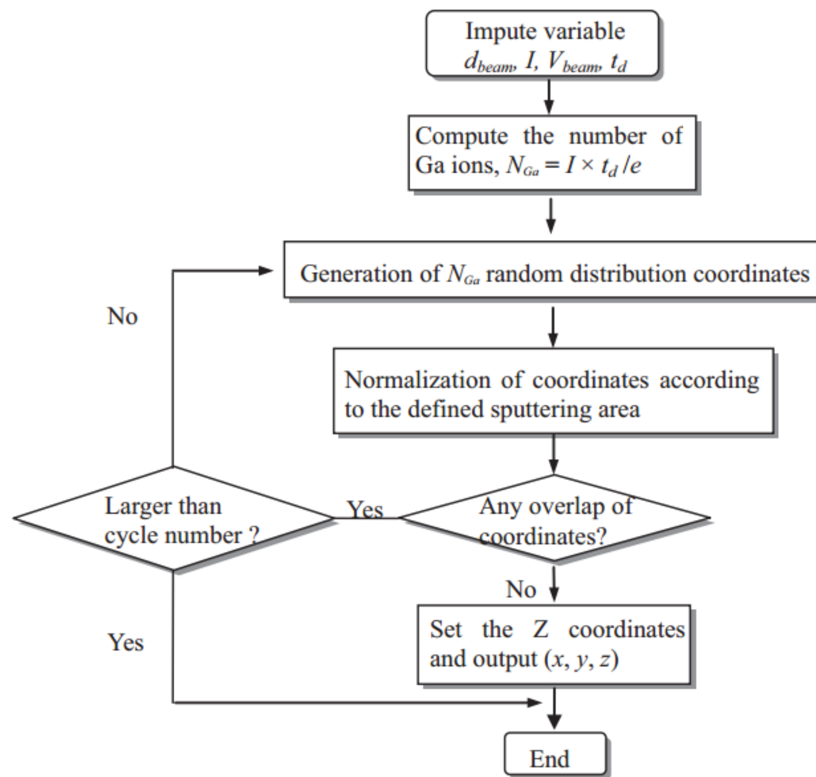

Figure 12: The program flowchart for building the multi-particle collision model [68].

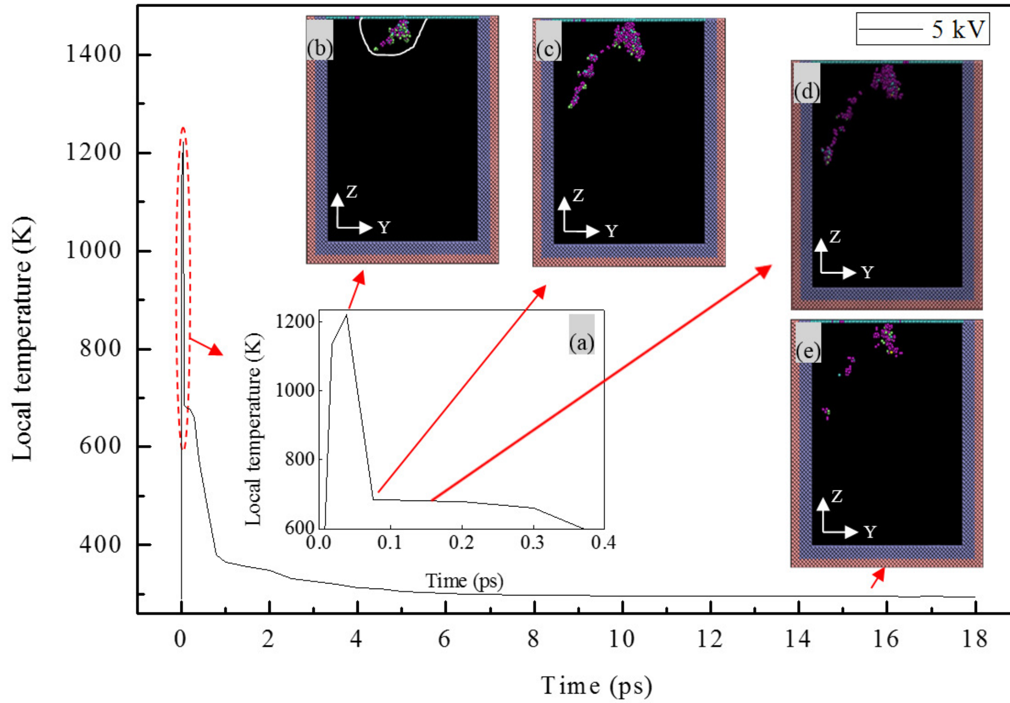

Figure 13: Molecular dynamics simulations describing the temperature evolution and the recrystallization process for the single Ga particle collision of diamond. Inset (a): the local view of the temperature during the temperature spike phase. Inset (b): the initial defects created when the local temperature has reached the peak value of 1221.2 K at 0.036 ps; this highest temperature region is shown by the encircled line. Inset (c): the defect configuration at the stage of the peak disorder of the lattice achieved at 0.094 ps. Inset (d): an intermediate phase during the recrystallization process observed at 0.15 ps; Ga particle stopped inside the diamond bulk at this stage. Inset (e): the residual atomic defects after the system cooled down to 293 K at 18.0 ps. The cyan atoms represent the dangling bonded C atoms and purple atoms represent sp^2 bonded C atoms. The C atoms of perfect diamond structure are removed from the visualizations [68].

4 Challenges in ion-induced damage study

The previous research work has provided a systematic analysis of ion-induced damage in diamond. However, due to the challenges involved in fabricating large, flat, and uniform TEM

samples in undoped non-conductive diamond, particularly the beam drift caused by electrostatic charging of diamond, the experimental research on the FIB-induced damage in single crystal diamond is limited. Moreover, in a typical FIB irradiation experiment, only ion dose is measurable during the test. The attempts to detect phase transformation that might occur during FIB processing diamond, are often disconnected from physical observations. The post-facto-observation leaves a gap in understanding the formation process of ion-induced damage, forcing the use of assumptions. In many cases, the average results measured by experiments will hide the fact of dynamic damage processes in target materials under different irradiation conditions. In contrast, MD simulations of ion bombardment have shed much light on ion beam mixing for decades. These activities make it an interesting and important task to understand what the fundamental effects of energetic particles on matter are.

5 Acknowledgements

The authors gratefully acknowledge the financial support from EPSRC (EP/K018345/1) and (EP/I033424/1), and the National Natural Science Foundation of China (no. 51575138) and (no. 51535003). Portions of this work were presented and published in thesis form in fulfilment of the requirements for the PhD from University of Strathclyde. The authors would also like to acknowledge the suggestions of the reviewers for helping improve the quality of this review paper.

6 References

[1] Ziegler, J.F., SRIM-2003. *Nucl. Instrum. Methods Phys. Res., Sect. B*, **2004**, 219, 1027–1036.

[2] Bhavsar, S.N., S. Aravindan, and P.V. Rao. A critical review on microtools fabrication by focused ion beam (FIB) technology, *Proc. of the World Congress on Eng.*, 2009, pp. 1510–1515.

[3] Orwa, J.; Nugent, K.; Jamieson, D.; Prawer, S., Raman investigation of damage caused by deep ion implantation in diamond. *Phys. Rev. B*, **2000**, 62(9), 5461.

[4] Brunetto, R., Baratta, G. A., and Strazzulla, G., Amorphization of diamond by ion

irradiation: a Raman study, *J. Phys.: Conference Series,* **2005**, pp. 120.

[5] Khomich, A.; Khmelnitskiy, R.; Dravin, V.; Gippius, A.; Zavedeev, E.; Vlasov, I., Radiation damage in diamonds subjected to helium implantation. *Phys. Solid State*, **2007**, 49(9), 1661–1665.

[6] Popok, V.; Samela, J.; Nordlund, K.; Popov, V., Implantation of keV-energy argon clusters and radiation damage in diamond. *Phys. Rev. B*, **2012**, 85(3), 033405.

[7] Dantelle, G.; Slablab, A.; Rondin, L.; Lainé, F.; Carrel, F.; Bergonzo, P.; Perruchas, S.; Gacoin, T.; Treussart, F.; Roch, J.F., Efficient production of NV colour centres in nanodiamonds using high-energy electron irradiation. *J. Lumin.,* **2010**, 130(9), 1655–1658.

[8] McKenzie, W.; Quadir, M. Z.; Gass, M.; Munroe, P., Focused ion beam implantation of diamond. *Diamond Relat. Mater.*, **2011**, 20(8), 1125–1128.

[9] Rubanov, S.; Suvorova, A., Ion implantation in diamond using 30keV Ga^+ focused ion beam. *Diamond Relat. Mater.,* **2011**, 20(8), 1160–1164.

[10] Mayer, J.; Giannuzzi, L. A.; Kamino, T.; Michael, J., TEM sample preparation and FIB-induced damage. *Mrs Bull.*, **2007**, 32(05), 400–407.

[11] Campbell, B.; Mainwood, A., Radiation damage of diamond by electron and gamma irradiation. *Phys. Status Solidi A*, **2000**, 181(1), 99–107.

[12] Lohstroh, A.; Sellin, P.; Gkoumas, S.; Al-Barakaty, H.; Veeramani, P.; Özsan, M.; Prekas, G.; Veale, M.; Parkin, J.; Davies, A., The effect of fast neutron irradiation on the performance of synthetic single crystal diamond particle detectors. *Diamond Relat. Mater.,* **2010**, 19(7), 841–845.

[13] Schwartz, J.; Aloni, S.; Ogletree, D. F.; Schenkel, T., Effects of low-energy electron irradiation on formation of nitrogen–vacancy centers in single-crystal diamond. *New J. Phys.,* **2012**, 14(4), 043024.

[14] Newton, R.; Davidson, J.; Lance, M., Raman microscopic characterization of proton-irradiated polycrystalline diamond films. *Diamond Relat. Mater.,* **2005**, 14(2), 173–178.

[15] Hamada, M.; Teraji, T.; Ito, T., Field-induced effects of implanted Ga on high electric field diamond devices fabricated by focused ion beam. *Appl. Surf. Sci. ,* **2003**, 216(1), 65–71.

[16] Lardon, P.; Mer, C.; Delacour, P.; Bazin, B.; Tromson, D.; Normand, S.; Nesladek, M.; Foulon, F.; Bergonzo, P., Investigations of high quality diamond detectors for neutron fluency monitoring in a nuclear reactor. *Diamond Relat. Mater.,* **2006**, 15(4), 815–821.

[17] Bartolo, P.; Kruth, J.P.; Silva, J.; Levy, G.; Malshe, A.; Rajurkar, K.; Mitsuishi, M.; Ciurana, J.; Leu, M., Biomedical production of implants by additive electro-chemical and physical processes. *CIRP Annu. Manuf. Technol.,* **2012**, 61(2), 635–655.

[18] Jain, I.; Agarwal, G., Ion beam induced surface and interface engineering. *Surf. Sci. Rep.,* **2011**, 66(3), 77–172.

[19] Adams, D.; Vasile, M.; Mayer, T.; Hodges, V., Focused ion beam milling of diamond: effects of H 2 O on yield, surface morphology and microstructure. *J. Vac. Sci. Technol., B: Microelectronics and Nanometer Structures,* **2003**, 21(6), 2334–2343.

[20] Tong, Z.; Luo, X., Investigation of focused ion beam induced damage in single crystal diamond tools. *Appl. Surf. Sci. ,* **2015**, 347, 727–735.

[21] Tong, Z.; Luo, X.; Sun, J.; Liang, Y.; Jiang, X., Investigation of a scale-up manufacturing approach for nanostructures by using a nanoscale multi-tip diamond tool. *Int J Adv Manuf Technol,* **2015**, 80, 699–710.

[22] Gnaser, H.; Reuscher, B.; Brodyanski, A., Focused ion beam implantation of Ga in nanocrystalline diamond: Fluence-dependent retention and sputtering. *Nucl. Instrum. Methods Phys. Res., Sect. B,* **2008**, 266(8), 1666–1670.

[23] Philipp, P.; Bischoff, L., Investigation of conducting nano-structures on ta-C films made by FIB lithography. *Nucl. Instrum. Methods Phys. Res., Sect. B,* **2012**, 282, 121–124.

[24] Unocic, K. A.; Mills, M. J.; Daehn, G. S., Effect of gallium focused ion beam milling on preparation of aluminium thin foils. *J. Microsc.*, **2010**, 240(3), 227–238.

[25] Kupfer, B. Z.; Ahmad, R. K.; Zainal, A.; Jackman, R. B., Fabrication and characterisation of triangle-faced single crystal diamond micro-cantilevers. *Diamond Relat. Mater.,* **2010**, **19**(7), 742–747.

[26] Wu, W.; Xu, Z.; Fang, F.; Liu, B.; Xiao, Y.; Chen, J.; Wang, X.; Liu, H., Decrease of FIB-induced lateral damage for diamond tool used in nano cutting. *Nucl. Instrum. Methods Phys. Res., Sect. B,* **2014**, 330, 91–98.

[27] Kawasegi, N.; Niwata, T.; Morita, N.; Nishimura, K.; Sasaoka, H., Improving machining performance of single-crystal diamond tools irradiated by a focused ion beam. *Precision Eng.,* **2014**, 38(1), 174–182.

[28] Buckmaster, R.; Hanada, T.; Kawazoe, Y.; Cho, M.-w.; Yao, T.; Urushihara, N.; Yamamoto, A., Novel Method for Site-Controlled Surface Nanodot Fabrication by Ion Beam Synthesis. *Nano Lett.,* **2005**, 5(4), 771–776.

[29] Bukonte, L.; Djurabekova, F.; Samela, J.; Nordlund, K.; Norris, S.; Aziz, M., Comparison of molecular dynamics and binary collision approximation simulations for atom displacement analysis. *Nucl. Instrum. Methods Phys. Res., Sect. B,* **2013**, 297, 23–28.

[30] Nordlund, K., Molecular dynamics simulation of ion ranges in the 1–100 keV energy range. *Comput. Mater. Sci.,* **1995**, 3(4), 448–456.

[31] Robinson, M. T.; Torrens, I. M., Computer simulation of atomic-displacement cascades in solids in the binary-collision approximation. *Phys. Rev. B,* **1974**, 9(12), 5008.

[32] Kim, H.B.; Hobler, G.; Lugstein, A.; Bertagnolli, E., Simulation of ion beam induced micro/nano fabrication. *J. Micromech. and Microeng.,* **2007**, 17(6), 1178.

[33] Robinson, M. T.; Torrens, I. M., Computer simulation of atomic-displacement cascades in solids in the binary-collision approximation. *Nucl. Instrum. Methods Phys. Res., Sect. B,* **1992**, 67(1), 396–400.

[34] Posselt, M.; Biersack, J., Computer simulation of ion implantation into crystalline targets. *Nucl. Instrum. Methods Phys. Res., Sect. B*, **1992**, 64(1), 706–710.

[35] Posselt, M., Crystal-TRIM and its application to investigations on channeling effects during ion implantation. *Radiat Eff. Defects Solids,* 1994, 130(1), 87–119.

[36] Nordlund, K.; Djurabekova, F., Multiscale modelling of irradiation in nanostructures. *J.*

Comput. Electron., **2014**, 13(1), 122–141.

[37] Backman, M.; Djurabekova, F.; Pakarinen, O. H.; Nordlund, K.; Zhang, Y.; Toulemonde, M.; Weber, W. J., Cooperative effect of electronic and nuclear stopping on ion irradiation damage in silica. *J. Phys. D: Appl. Phys.*, **2012**, 45(50), 505305.

[38] Backman, M.; Toulemonde, M.; Pakarinen, O. H.; Juslin, N.; Djurabekova, F.; Nordlund, K.; Debelle, A.; Weber, W. J., Molecular dynamics simulations of swift heavy ion induced defect recovery in SiC. *Comput. Mater. Sci.,* **2013**, 67, 261–265.

[39] Tersoff, J., New empirical approach for the structure and energy of covalent systems. *Phys. Rev. B*, **1988**, 37(12), 6991.

[40] Nordlund, K., Atomistic simulation of radiation effects in carbon-based materials and nitrides. *Nucl. Instrum. Methods Phys. Res., Sect. B,* **2004**, 218, 9–18.

[41] Henriksson, K. O.; Vörtler, K.; Dreißigacker, S.; Nordlund, K.; Keinonen, J., Sticking of atomic hydrogen on the tungsten (001) surface. *Surf. sci.,* **2006**, 600(16), 3167–3174.

[42] Nordlund, K., Computational materials science of ion irradiation. *Nucl. Instrum. Methods Phys. Res., Sect. B*, **2002**, 188(1), 41–48.

[43] Alder, B.; Wainwright, T., Phase transition for a hard sphere system. *The J. Chem. Phys.,* **1957**, 27(5), 1208–1209.

[44] Brinkman, J. A., On the nature of radiation damage in metals. *J. Appl. Phys.,* **1954**, 25(8), 961-970.

[45] Averback, R., Atomic displacement processes in irradiated metals. *J. Nucl. Mater.,* **1994**, 216, 49–62.

[46] Harrison Jr, D. E., Application of molecular dynamics simulations to the study of ion-bombarded metal surfaces. *Crit. Rev. Solid State Mater. Sci.,* **1988**, 14(S1), s1–s78.

[47] De La Rubia, T. D.; Averback, R. S.; Benedek, R.; King, W., Role of thermal spikes in energetic displacement cascades. *Phys. Rev. letts,* **1987**, 59(17), 1930.

[48] Bacon, D.; Calder, A.; Gao, F.; Kapinos, V.; Wooding, S., Computer simulation of defect production by displacement cascades in metals. *Nucl. Instrum. Methods Phys. Res., Sect. B,* **1995**, 102(1), 37–46.

[49] Caturla, M.; Diaz de la Rubia, T.; Gilmer, G. H., Disordering and defect production in silicon by keV ion irradiation studied by molecular dynamics. *Nucl. Instrum. Methods Phys. Res., Sect. B,* **1995**, 106(1), 1-8.

[50] Gades, H.; Urbassek, H. M., Dimer emission in alloy sputtering and the concept of the “clustering probability”. *Nucl. Instrum. Methods Phys. Res., Sect. B*, **1995**, 103(2), 131–138.

[51] Phythian, W.; Stoller, R.; Foreman, A.; Calder, A.; Bacon, D., A comparison of displacement cascades in copper and iron by molecular dynamics and its application to microstructural evolution. *J. Nucl. Mater.*, **1995**, 223(3), 245–261.

[52] Ghaly, M.; Averback, R.; Diaz De La Rubia, T., Surface effects on damage production during ion bombardment: A molecular dynamics study. *Nucl. Instrum. Methods Phys. Res., Sect. B,* **1995**, 102(1), 51–57.

[53] Gilmer, G.; Diaz de la Rubia, T.; Stock, D.; Jaraiz, M., Diffusion and interactions of point defects in silicon: Molecular dynamics simulations. *Nucl. Instrum. Methods Phys. Res., Sect. B,* **1995**, 102(1), 247–255.

[54] Nordlund, K.; Averback, R., Point defect movement and annealing in collision cascades. *Phys. Rev. B,* **1997**, 56(5), 2421.

[55] Nord, J.; Nordlund, K.; Keinonen, J., Amorphization mechanism and defect structures in ion-beam-amorphized Si, Ge, and GaAs. *Phys. Rev. B,* **2002**, 65(16), 165329.

[56] Saada, D.; Adler, J.; Kalish, R., Transformation of Diamond (sp3) to Graphite (sp2) Bonds by Ion-Impact. *Int. J. Mod Phys C*, **1998**, 9(01), 61–69.

[57] Saada, D.; Adler, J.; Kalish, R., Computer simulation of damage in diamond due to ion impact and its annealing. *Phys. Rev. B,* **1999**, 59(10), 6650.

[58] Kalish, R.; Reznik, A.; Nugent, K.; Prawer, S., The nature of damage in ion-implanted and annealed diamond. *Nucl. Instrum. Methods Phys. Res., Sect. B*, **1999**, 148(1), 626–633.

[59] Kalish, R.; Reznik, A.; Prawer, S.; Saada, D.; Adler, J., Ion-Implantation-Induced Defects in Diamond and Their Annealing: Experiment and Simulation. *Phys. Status Solidi A*, **1999**, 174(1), 83–99.

[60] Satake, S.I.; Inoue, N.; Taniguchi, J.; Shibahara, M. In *Molecular dynamics simulation for focused ion beam processing: a comparison between computational domain and potential energy*, *J. Phys.: Conference Series, IOP Publishing:* 2008; pp. 012013.

[61] Satake, S.I.; Momota, S.; Yamashina, S.; Shibahara, M.; Taniguchi, J., Surface deformation of Ar^+ ion collision process via molecular dynamics simulation with comparison to experiment. *J. Appl. Phys.*, **2009**, 106(4), 044910.

[62] Li, L.; Xu, M.; Song, W.; Ovcharenko, A.; Zhang, G.; Jia, D., The effect of empirical potential functions on modeling of amorphous carbon using molecular dynamics method. *Appl. Surf. Sci.* , **2013**, 286, 287–297.

[63] Smith, R.; Kenny, S. D.; Ramasawmy, D., Molecular-dynamics simulations of sputtering. *Philos. Trans. R. Soc. London, Ser. A*, **2004**, 362(1814), 157–176.

[64] Satake, S.I.; Momota, S.; Fukushige, A.; Yamashina, S.; Shibahara, M.; Taniguchi, J., Molecular dynamics simulation of surface deformation via Ar^+ ion collision process. *Nucl. Instrum. Methods Phys. Res., Sect. B*, **2012**, 272, 5–8.

[65] Li, X.; Ke, P.; Lee, K.-R.; Wang, A., Molecular dynamics simulation for the influence of incident angles of energetic carbon atoms on the structure and properties of diamond-like carbon films. *Thin Solid Films,* **2014**, 552, 136–140.

[66] Sasajima, Y.; Akabane, T.; Nakazawa, T.; Iwase, A., Computer simulation of high-energy-beam irradiation of single-crystalline silicon. *Nucl. Instrum. Methods Phys. Res., Sect. B,* **2007**, 264(2), 259–266.

[67] Silverman, A.; Adler, J.; Kalish, R., Diamond membrane surface after ion-implantation-induced graphitization for graphite removal: Molecular dynamics simulation. *Phys. Rev. B*, **2011**, 83(22), 224206.

[68] Tong, Z.; Xu, Z.; Wu, W.; Luo, X., Molecular dynamic simulation of low-energy FIB irradiation induced damage in diamond. *Nucl. Instrum. Methods Phys. Res., Sect. B*, **2015**,

358, 38–44.

[69] Jorgensen, W. L.; Chandrasekhar, J.; Madura, J. D.; Impey, R. W.; Klein, M. L., Comparison of simple potential functions for simulating liquid water. *The J. Chem. Phys.*, **1983**, 79(2), 926–935.

[70] Verlet, L., Computer" experiments" on classical fluids. I. Thermodynamical properties of Lennard-Jones molecules. *Phys. Rev.*, **1967**, 159(1), 98.

[71] Ikawa, N.; Shimada, S.; Tanaka, H.; Ohmori, G., An atomistic analysis of nanometric chip removal as affected by tool-work interaction in diamond turning. *CIRP Annu. Manuf. Technol.,* **1991**, 40(1), 551–554.

[72] Girifalco, L. A.; Weizer, V. G., Application of the Morse potential function to cubic metals. *Phys. Rev*., **1959**, 114(3), 687.

[73] Tersoff, J., Modeling solid-state chemistry: Interatomic potentials for multicomponent systems. *Phys. Rev. B*, **1989**, 39(8), 5566.

[74] Daw, M. S.; Foiles, S. M.; Baskes, M. I., The embedded-atom method: a review of theory and applications. *Mate. Sci. Rep.,* **1993**, 9(7), 251–310.

[75] Cleri, F.; Rosato, V., Tight-binding potentials for transition metals and alloys. *Phys. Rev. B,* **1993**, 48(1), 22.

[76] Satake, S.; Inoue, N.; Kunugi, T.; Shibahara, M.; Kasahara, H., Large-scale molecular dynamics simulation for two Ar clusters impact on 4H–SiC. *Nucl. Instrum. Methods Phys. Res., Sect. B*, **2007**, 257(1), 639–644.

[77] Burenkov, A.; Sekowski, M.; Belko, V.; Ryssel, H., Angular distributions of sputtered silicon at grazing gallium ion beam incidence. *Nucl. Instrum. Methods Phys. Res., Sect. B*, **2012**, 272, 23–27.

[78] Russo Jr, M. F.; Maazouz, M.; Giannuzzi, L. A.; Chandler, C.; Utlaut, M.; Garrison, B. J., Trench formation and lateral damage induced by gallium milling of silicon. *Appl. Surf. Sci. ,* **2008**, 255(4), 828–830.